

# Catalysis Science & Technology

Accepted Manuscript



This is an *Accepted Manuscript*, which has been through the Royal Society of Chemistry peer review process and has been accepted for publication.

*Accepted Manuscripts* are published online shortly after acceptance, before technical editing, formatting and proof reading. Using this free service, authors can make their results available to the community, in citable form, before we publish the edited article. We will replace this *Accepted Manuscript* with the edited and formatted *Advance Article* as soon as it is available.

You can find more information about *Accepted Manuscripts* in the [Information for Authors](#).

Please note that technical editing may introduce minor changes to the text and/or graphics, which may alter content. The journal's standard [Terms & Conditions](#) and the [Ethical guidelines](#) still apply. In no event shall the Royal Society of Chemistry be held responsible for any errors or omissions in this *Accepted Manuscript* or any consequences arising from the use of any information it contains.



## Catalysis Science &amp; Technology

## ARTICLE

## Enhancing the hydrogen transfer catalytic activity of hybrid carbon nanotube-based NHC-iridium catalysts by increasing the oxidation degree of the nanosupport

Received 00th January 20xx,  
Accepted 00th January 20xx

DOI: 10.1039/x0xx00000x

www.rsc.org/

Matías Blanco,<sup>a</sup> Patricia Álvarez,<sup>a</sup> Clara Blanco,<sup>a</sup> M. Victoria Jiménez<sup>\*b</sup>, Jesús J. Pérez-Torrente,<sup>b</sup> Luis A. Oro,<sup>b</sup> Javier Blasco,<sup>c</sup> Vera Cuartero,<sup>d</sup> and Rosa Menéndez<sup>\*a</sup>

CVD-grown multiwalled carbon nanotubes were purified applying four different treatments with increasing oxidation severity. The growing severity of the treatment results in a progressive oxygen functionalization of the surface along with introduction of an increasing quantity of defects on the carbon nanotubes walls. Iridium N-heterocyclic carbene complexes were covalently anchored to those oxidized surfaces through their surface carboxylic acids via acetyl linkers. The carbon nanotube-based iridium-NHC hybrid materials developed are active in the hydrogen-transfer reduction of cyclohexanone to cyclohexanol with 2-propanol/KOH as hydrogen source but with rather different activity. The catalytic activity of the hybrid catalysts is strongly influenced by the type and amount of oxygenated functionalization resulting from the treatment applied to the support, being the most active the most oxidized material.

### 1. Introduction

N-Heterocyclic carbenes (NHCs) have attracted increasing attention as ancillary ligands for the design of transition metal homogeneous catalysts.<sup>1</sup> On one hand, the tuneable character of NHC ligands allows for the control of the sterical and electronic properties at the metal centre.<sup>2</sup> On the other hand, organometallic catalysts can be anchored on solid supports through the wingtip of the NHC ligand with potential improvement of the catalytic activity by support effects permitting, additionally, the easy recovery and subsequent recyclability of the hybrid catalysts.<sup>3,4</sup>

Carbon nanotubes (CNT),<sup>5</sup> among other carbon materials, present excellent electronic, thermal, chemical and mechanical properties<sup>6,7,8</sup> which make them suitable to support molecular transition metal complexes. All the synthetic methods used in their

production, *i.e.* arc discharge, laser vaporization or CVD,<sup>9</sup> result in impurities that join every produced CNT batch, which are mainly based on amorphous carbon particles and traces of the metals employed for the growth of the nanotubes.<sup>10</sup> Purification methods involve thermal annealing, electrochemical or magnetic treatments, but the most applied procedures are based on different acid/oxidant treatments in order to dissolve the metals and eliminate the carbon impurities.<sup>11</sup> It is known that these treatments also affect the carbon walls of the CNTs. In fact, the oxidation surface chemistry of CNTs is reasonably well-established,<sup>12</sup> and surface oxygen groups are deployed after the purification by oxidation processes, mainly carboxylic acids on the edges, tips and defects, and hydroxylic and epoxy groups on the basal planes.<sup>13</sup> depending on the grade of oxidation.<sup>14,15,16</sup> Several proposals about the mechanism involving the oxidation of the CNTs walls have been reported in the literature, but all of them agree that the severity of the treatments directly relates with the degree of oxidation.

Iridium-NHC complexes are efficient catalyst precursors for the reduction of C=O and C=N bonds to generate alcohols or amines under mild transfer hydrogenation conditions.<sup>17,18,19</sup> The covalent immobilization of Ir-NHC complexes on CNTs can be achieved taking advantage of their oxygenated surface chemistry but their development as hybrid catalysts is under expansion in comparison with other suitable supports.<sup>20</sup> In this regard, we have developed synthetic protocols for the covalent immobilization of Ir-NHC complexes to carbon surfaces through the carboxylic acid or the

<sup>a</sup> Instituto Nacional del Carbón INCAR-CSIC, P.O. Box 73, 33080, Oviedo, Spain. [rosmenen@incar.csic.es](mailto:rosmenen@incar.csic.es)

<sup>b</sup> Department of Inorganic Chemistry, Instituto de Síntesis Química y Catálisis Homogénea (ISQCH-CSIC). University of Zaragoza, 50009, Zaragoza Spain. [vjimenez@unizar.es](mailto:vjimenez@unizar.es)

<sup>c</sup> Instituto de Ciencia de Materiales de Aragón-ICMA, Departamento de Física de la Materia Condensada, CSIC-Universidad de Zaragoza, 50009 Zaragoza, Spain.

<sup>d</sup> ESRF-The European Synchrotron, 71, Avenue des Martyrs, Grenoble, France

Electronic Supplementary Information (ESI) available: [details of any supplementary information available should be included here]. See DOI: 10.1039/x0xx00000x

hydroxyl surface groups by using hydroxy-functionalized imidazolium salt. This functionalization approach result in the formation of ester and carbonate functions, respectively, as linkers to the Ir-NHC species. Interestingly, the hybrid materials were found to be efficient hydrogen-transfer catalysts exhibiting good recyclability.

The aim of this work is the covalently anchoring of Ir-NHC complexes, via acetyl linkers, through the carboxylic acids of different oxidized CNTs supports resulting from oxidizing treatments of increasing severity. We are aware that only a few N-acyl-substituted NHCs transition metal complexes have been reported up to date.<sup>21</sup> In addition, it has been found that these complexes usually react quickly and irreversible with a great variety of mild nucleophiles, including water and alcohols, to give the corresponding protic NHC complexes.<sup>21a</sup> However, to our delight, we have found that these iridium hybrid catalysts exhibit an outstanding catalytic activity in hydrogen transfer, which is probably a consequence of the stabilizing effect exerted by the carbon nanotube support. Thus, the catalytic activity, stability and recyclability of the resultant hybrid materials in transfer hydrogenation reactions have been studied as a function of the surface chemistry of their corresponding support. In this context, it is worth noting that detailed catalytic studies based on supported catalysts with a gradual oxidation level of their surfaces are scarce.

## 2. Experimental

### Materials

All the chemicals, including starting multiwalled carbon nanotubes, were purchased from Aldrich. Reagent or HPLC grade were employed in all the experiments. Solvents were distilled immediately prior to use from the appropriate drying agents or obtained from a Solvent Purification System (Innovative Technologies). The starting organometallic compound  $[\text{Ir}(\mu\text{-OMe})(\text{cod})_2]$  ( $\text{cod} = 1,5\text{-cyclooctadiene}$ ) was prepared according to standard literature procedure.<sup>22</sup>

### Oxidation of the carbon nanotubes

Carbon nanotubes were subjected to four different purification treatments of increasing severity: (a) 0.3 g of raw carbon nanotubes was dispersed in 70 mL of concentrated HCl. The mixture was magnetically stirred at 60 °C for 2 h. The suspension was washed by addition of several portions of 250 mL of water, centrifugation, and elimination of the supernatant till neutral pH was reached. The solid collected was dried at 100 °C until constant weight, and labelled as **CNT-HCl**. (b) 0.3 g of raw carbon nanotubes was dispersed in 25 mL of a 1:1 mixture of ammonium hydroxide (28%) and hydrogen peroxide (30%). The mixture was magnetically stirred at 80 °C for 5 h and then the washing procedure described above was applied till

neutral pH. The solid was dried and labelled as **CNT-LT**. (c) 0.3 g of raw CNT was dispersed in 70 mL of a solution of nitric acid 3 M. The mixture was magnetically stirred at 60 °C for 15 min, sonicated for 2 h and then diluted with 250 mL of water. After centrifugation, the washing procedure with water was repeated till neutral pH as in the precedent preparations. The collected solid was dispersed in 70 mL of hydrogen peroxide (30%) and the mixture magnetically stirred at 60 °C for 15 min, and then sonicated for 2 h. The solid was collected by filtration, washed with water and dried over 100 °C until constant weight. The dried solid obtained was named as **CNT-MT**. (d) 0.3 g of raw CNT was dispersed in 40 mL of a 3:1 mixture of concentrated sulphuric and nitric acid. The mixture was sonicated for 10 min, magnetically stirred at 80 °C for 20 min and then sonicated for another 20 min. Finally, it was diluted with 250 mL of water, and after centrifugation, the standard washing procedure with water was repeated till neutral pH as in the precedent preparations. The solid was dried over 100 °C until constant weight, and named as **CNT-ST**.

### Covalent functionalization of the carbon nanotubes

The cationic iridium complexes bearing methyl imidazol-2-ylidene ligands were anchored to the oxidized carbon nanotubes through acetyl functions applying a three-step procedure. 100 mg of **CNT-X** was refluxed in 40 mL of thionyl chloride for 24 h under an argon atmosphere. The excess of  $\text{SOCl}_2$  was removed under vacuum and the resultant product washed three times with 20 mL of tetrahydrofuran (THF) and dried for 2 h under vacuum. Then, the solid was dispersed in 15 mL of THF and N-methylimidazole (2 mL, 25.1 mmol) was added. The mixture was refluxed for 24 h. The solid was filtered, and washed with THF (3 × 20 mL), dichloromethane (3 × 20 mL) and diethyl ether (2 × 20 mL). The solids collected were dried at 100 °C in a preheated furnace for 2 h and the dried samples labelled as **CNT-X-MI**. The resulting imidazolium functionalized carbon nanotubes (100 mg) were reacted with  $[\text{Ir}(\mu\text{-OMe})(\text{cod})_2]$  (100 mg, 0.150 mmol) in THF (20 mL) under argon atmosphere. The mixtures were refluxed for 2 days and then immersed in an ultrasonic bath for 30 min at room temperature. The resultant solids were recovered by centrifugation, washed with THF (5 × 10 mL) and diethyl ether (2 × 5 mL), and dried under vacuum. The hybrid materials were labelled as **CNT-X-MI-Ir**, where X relates with the degree of oxidation of the nanotube (HCl, LT, MT and ST).

**Preparation of 1-acetyl-3-methyl-1H-imidazol-3-ium chloride.** Acetyl chloride (1.77 mL, 25 mmol) was added to a solution of N-methylimidazole (1.00 mL, 12.5 mmol) in acetonitrile (15 mL) and the mixture refluxed for 24 h. The white solid formed was separated by decantation, washed with diethyl ether and dried in vacuo. Yield: 63 %. <sup>1</sup>H NMR (298 K,  $\text{CDCl}_3$ ):  $\delta$  12.34 (s, 1H, NCHN), 7.88 (s, 1H, CH Im), 7.43 (s, 1H, CH Im), 4.30 (s, 3H,  $\text{NCH}_3$ ), 3.11 (s, 3H,  $\text{OCC}_3$ ).

**Reaction of  $[\{\text{Ir}(\mu\text{-OMe})(\text{cod})_2\}]_2$  with 1-acetyl-3-methyl-1H-imidazol-3-ium chloride.**  $[\{\text{Ir}(\mu\text{-OMe})(\text{cod})_2\}]_2$  (0.100 g, 0.151 mmol) was added to a suspension of the N-acetyl imidazolium salt (0.048 g, 0.302

mmol) in dry tetrahydrofuran (15 mL) containing activated molecular sieves. The mixture was stirred for 12 h at room temperature to give an orange suspension. The solids were removed by filtration and the resulting orange solution was evaporated to dryness under vacuum. The residue was treated with pentane to afford an orange solid, which was separated by decantation and dried in vacuo. The NMR of this solid showed that is actually a mixture of the complexes [IrCl(cod)(MelmCOCH<sub>3</sub>)] and [IrCl(cod)(MelmH)] in which the later predominates. Addition of dry methanol to a solution of this solid in C<sub>6</sub>D<sub>6</sub> resulted in the clean formation of [IrCl(cod)(MelmH)].

**[IrCl(cod)(MelmCOCH<sub>3</sub>)]**. <sup>1</sup>H NMR (298 K, C<sub>6</sub>D<sub>6</sub>): δ 7.32 (d, *J* = 2.3, 1H, CH Im), 5.85 (d, *J* = 2.3, 1H, CH Im), 5.17 (m, 1H CH cod), 5.09 (m, 1H, CH cod), 3.58 (s, 3H, CH<sub>3</sub> Im), 3.56 (m, 1H, CH cod), 3.52 (s, 3H, COCH<sub>3</sub>), 3.50 (m, 1H, CH cod), 2.58, 2.16, 2.03, 1.69 (m, 2:2:2:2, 8H, CH<sub>2</sub> cod). <sup>13</sup>C{<sup>1</sup>H} NMR (298 K, C<sub>6</sub>D<sub>6</sub>): δ 186.43 (NCN), 170.63 (CO), 122.24, 118.39 (CH Im), 85.86, 84.70, 52.22, 51.52 (CH cod), 38.45 (CH<sub>3</sub> Im), 33.89, 33.24, 29.75, 29.67 (CH<sub>2</sub> cod), 28.12 (COCH<sub>3</sub>).

**[IrCl(cod)(MelmH)]**. <sup>1</sup>H NMR (298 K, C<sub>6</sub>D<sub>6</sub>): δ 8.30 (br, 1H, NH), 6.82 (m, 1H, CH Im), 5.81 (m, 1H, CH Im), 5.00, 3.71 (m, 2:2, 4H CH cod), 2.38 (m, 4H, CH<sub>2</sub> cod), 2.19 (s, 3H, CH<sub>3</sub> Im), 1.70, 1.55 (m, 2:2, 4H CH<sub>2</sub> cod). <sup>13</sup>C{<sup>1</sup>H} NMR (298 K, C<sub>6</sub>D<sub>6</sub>): δ 182.18 (NCN), 126.0, 120.31 (CH Im), 66.80, 56.64 (CH cod), 32.98 (CH<sub>3</sub> Im), 32.42, 31.60 (CH<sub>2</sub> cod).

#### General procedure for the transfer hydrogenation catalysis

The catalytic transfer hydrogenation reactions were carried out under argon atmosphere in thick glass reaction tubes fitted with a greaseless high-vacuum stopcock. In a typical experiment, the reactor was charged with a solution of cyclohexanone (0.52 mL, 5.0 mmol) in 2-propanol (4.5 mL), internal standard (mesitylene, 70 μL, 0.5 mmol), base (0.1 mL, 0.025 mmol of a KOH solution 0.24 M in 2-propanol) and the catalyst (0.005 mmol, 0.1 mol %). The resulting mixture was stirred at room temperature for 10 min and then placed in a thermostatic oil bath at the required temperature, typically 80 °C. Conversions were determined by gas chromatography analysis under the following conditions: column temperature of 35 °C (2 min) up to 220 °C at 10 °C min<sup>-1</sup>, and a flow rate of 1 mL min<sup>-1</sup> using ultrapure He as carrier gas. Once the reaction was completed, the hybrid iridium-NHC catalysts were recovered by centrifugation and washed with additional amounts of 2-propanol (3 x 10 mL). Several catalytic cycles were performed with these materials, under the same experimental conditions, without adding any fresh catalyst precursor. The last cycle was carried out in air.

#### Characterization methods

The catalytic reactions were analysed on an Agilent 4890 D system equipped with an HP-INNOWax capillary column (0.4 μm, 25 m x 0.2

mm i.d.) using mesitylene as internal standard. Thermogravimetric analysis (TGA) of the materials was performed on a TA SDT 2960 analyzer thermobalance. The procedure used was as follows: 3 mg of sample was heated in the thermobalance at 10 °C min<sup>-1</sup> to 1000 °C using a nitrogen flow of 200 mL min<sup>-1</sup>. Raman spectra of the parent oxidized nanotubes and the imidazolium-modified materials were recorded from 750 to 3500 cm<sup>-1</sup> on a Renishaw 2000 Confocal Raman Microprobe (Renishaw Instruments, England) using a 514.5 nm argon ion laser. Images of high-resolution transmission electron microscopy (HRTEM) were recorded using a JEOL JEM-2100F transmission electron microscope, equipped with a field-emission-gun (FEG) operating at 200 kV, and fitted with an Oxford Instruments microprobe to perform Energy-dispersive X-ray spectroscopy (EDX), in order to verify the atomic composition of the catalyst. The samples were prepared by casting a few drops of 1 mg mL<sup>-1</sup> ethanol suspensions of the materials over the carbon grids. To minimize exposure of the samples to the air, the suspensions were transferred to a lacey carbon grid using a glovebox filled with ultrahigh-purity argon and then to the TEM holder in order to minimize the time required to introduce them into the microscope. The X-ray photoemission spectroscopy (XPS) spectra were recorded using a SPECS system operating under a pressure of 10<sup>-7</sup> Pa and equipped with a Mg Kα X-ray source. The functional groups in the nanotube based materials were quantified by deconvolution of the high resolution C1s XPS peak employing Gaussian and Lorentzian functions.<sup>23</sup> The binding energy profiles were deconvoluted as follows: undamaged structures of sp<sup>2</sup>-hybridized carbon (284.5 eV), damaged structures or sp<sup>3</sup>-hybridized carbons (and C-N groups, 285.5 eV), C-O (and C-N groups, 286.5 eV), C=O functional groups (287.7 eV) and COO groups at 288.7 eV. The amount of iridium present in the samples was determined by means of Inductively Coupled Plasma Mass Spectrometry (ICP-MS) in an Agilent 7700x instrument. The samples were digested following a method described elsewhere.<sup>24</sup> Briefly, 30 mg of sample was treated with 5 mL of a mixture of concentrated nitric and hydrochloric acid (3:1 ratio) at 180 °C for 3 h under microwave irradiation.

X-ray absorption measurements at the Ir L<sub>3</sub>-edge were performed with a Si(111) double crystal monochromator at the BM23 beam line of the ESRF (Grenoble, France) and with a Si(311) one at the Claess beam line of the Alba (Barcelona, Spain) synchrotron facilities. Spectra collected from both setups were equivalent. The energy resolution δE/E was estimated about 8×10<sup>-5</sup> at the Ir L<sub>3</sub>-edge and a pellet of Ir metal and cellulose, the complex [IrCl(cod)(Melm(CH<sub>2</sub>)<sub>3</sub>OH)] and the salt IrCl<sub>3</sub> were simultaneously measured for energy calibration as references for Ir(0), Ir(I) and Ir(III), respectively. The extended X-ray absorption fine structure (EXAFS) spectra was analysed using the ARTEMIS program,<sup>25</sup> which makes use of theoretical phases and backscattering amplitudes calculated from FEFF6.<sup>26</sup> The fits were carried out in the R space using a Hanning window for filtering purposes.

### 3. Results and discussion

#### Preparation and functionalization of carbon nanotubes with different oxidation level

The carbon nanotube-based support materials, **CNT-X**, were obtained from commercial CVD-grown multiwalled carbon nanotubes applying different and gradually increasing oxidation reagents, that is: a) hydrochloric acid, b) a mixture of hydrogen

peroxide and ammonium hydroxide, c) diluted nitric acid and hydrogen peroxide and d) a mixture of warm concentrated sulphuric and nitric, acids.<sup>27</sup> It is noticeable that the ongoing oxidation processes on the CNTs generates oxygen functional groups at edges, defects and basal planes of the nanotubes. The quantity of defects observed on the carbon nanotubes walls of oxidized samples is directly proportional to the harshness of the oxidation treatment. In fact, a gradual increment in the D band of the Raman spectra is observed as a result of those treatments. Furthermore, the C/O atomic ratio calculated by XPS data (Table 1) also decreases gradually.

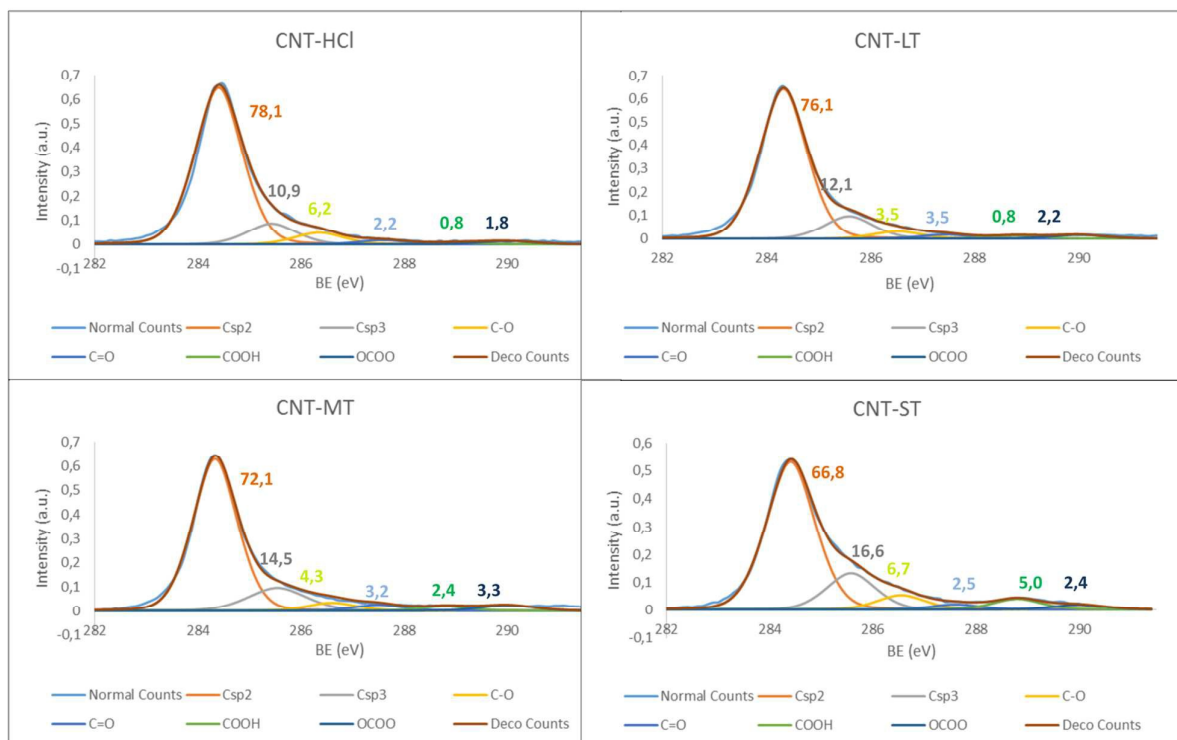


**Fig 1.** XPS C1s fitting of the parent materials **CNT-X**: a) **CNT-HCl**, b) **CNT-LT**, c) **CNT-MT** and d) **CNT-ST**.

The generated surface groups on the **CNT-X** materials were analysed by deconvolution of the C1s band in the XPS spectra (Fig. 1), what also confirm the progressive introduction of oxygen groups following the increase of oxidation severity. Additionally, the diminution in the Csp<sup>2</sup> band and the intensification in the Csp<sup>3</sup> are both consequences of those oxidation processes. Interestingly, in accordance with this argument, the most oxidized carbon nanotube material, **CNT-ST**, show the largest amount of carboxylic acids and hydroxylic groups. Additionally, the large percentage of oxygen in this material, also observed in graphene oxides, is also attributed to an increase in unreactive epoxy or ether groups.<sup>28</sup>

Applying a known carbon nanotube functionalization method, the treatment of the parent oxidized nanotubes (**CNT-X**) with thionyl chloride followed by reaction with N-methylimidazole allow the formation of hanging methylimidazolium salts by alkylation of the heterocycle with the more reactive pendant acyl groups. Operating in such a way, it is possible to obtain the imidazolium functionalized carbon nanotube materials named as **CNT-X-MI** (**MI** = 1-acyl-3-methylimidazolium, Scheme 1).

The high-resolution XPS N1s bands of the functionalized samples reveal a single band at 401.5 eV that is indicative of a unique functionalization mode. The atomic percentages obtained

from XPS data (Table 1) show a steady increase in the amount of nitrogen, which corresponds to an increasing functionalization of the carbon nanotube materials with the imidazolium groups. Also, a higher  $I_D/I_G$  Raman ratio was observed in every sample, and also when comparing the parent-oxidized with imidazole-treated materials, what indicates a positive functionalization, which is in accordance with the correlation observed in related materials (see the ESI).<sup>29</sup> In addition, the correct atomic ratio N:Cl of ca. 2:1 was obtained what is in agreement with the presence of the imidazole ring (see the ESI). All these data confirms that the more oxidizing treatment applied, the more functionalized support obtained, what is **CNT-ST-MI**.

The quantification of the imidazolium groups present in these materials has also been determined by means of thermogravimetric analysis (TGA) as the weight losses at 400 °C (mainly associated to the elimination of the imidazolium fragments).<sup>30</sup> As expected, more pronounced decays in the TGA profiles were observed for the materials coming from the more oxidized CNTs, what is in accordance with a larger number of imidazole units in these materials (see the ESI).<sup>26</sup> In fact, the nitrogen weight percentages determined from the TGA curves compares well with those obtained from XPS data (see the ESI).

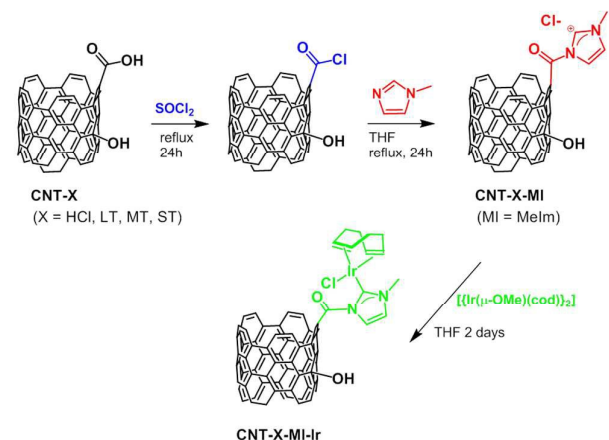
**Table 1.** XPS data of carbon nanotube-based support materials, imidazolium-functionalized carbon nanotube materials, and ICP analysis for the hybrid catalysts.

Sample	XPS (atom %)						ICP (wt %)
	C/O	C	Cl	N	O	S	
CNT-HCl	28	96.6	0.0	0.0	3.4	0.0	
CNT-HCl-MI	23	93.7	0.5	0.9	4.0	0.8	
CNT-HCl-MI-Ir							3.1
CNT-LT	20	95.2	0.0	0.0	4.8	0.0	
CNT-LT-MI	20	92.4	0.6	1.4	4.6	1.0	
CNT-LT-MI-Ir							6.1
CNT-MT	16	94.1	0.0	0.0	5.9	0.0	
CNT-MT-MI	15	91.4	0.8	1.7	6.1	0.0	
CNT-MT-MI-Ir							10.0
CNT-ST	4	80.8	0.0	0.0	19.2	0.0	
CNT-ST-MI	3.5	73.9	1.3	2.3	21.0	1.5	
CNT-ST-MI-Ir							12.3

#### Synthesis and characterization of carbon nanotube-NHC-iridium hybrid catalysts.

The deprotonation of the weak acid proton at the C2 of the supported imidazolium groups by the basic methoxy ligands in the dinuclear complex  $[\text{Ir}(\mu\text{-OMe})(\text{cod})_2]$  (cod = 1,5-cyclooctadiene) generate N-heterocyclic carbene (NHC) anchored iridium complexes (Scheme 1) on the nanotube surfaces, **CNT-X-MI-Ir**. The insolubility of these materials, together with the detection of methanol by gas chromatography in the filtered mother liquids after reaction with  $[\text{Ir}(\mu\text{-OMe})(\text{cod})_2]$  (see the ESI), confirm the progress of the reactions. The supporting of the metal complexes is substantiated by the high-resolution transmission electron microscopy images of the four types of Ir-NHC hybrid materials derived from gradually

oxidized carbon nanotubes (**CNT-X-MI-Ir**) showed in Fig. 2. Homogeneous distributions of electron-dense regions were detected with diameters ranging 0.15-0.3 nm all throughout outer and inner walls (white circles). The metallic spots are in the range of the molecular iridium complexes as was confirmed by their EDX spectra (see the ESI).



**Scheme 1.** Synthesis of carbon nanotube materials: from **CNT-X** to **CNT-X-MI-Ir**

Although larger iridium particles of 1.2-1.4 nm are also detected, the Ir4f region of the XPS spectra shows, for all samples, two maxima centred at 62.4 and 66.5 eV, corresponding to Ir4f<sub>7/2</sub> and Ir4f<sub>5/2</sub>, according to Ir(I) species.<sup>31</sup> Those larger spots, more marked on the unprotected outer walls, could be clusters or nanoparticles possibly formed by electron beam irradiation inside the microscope chamber.<sup>32</sup> Similar size distributions were observed for other supported molecular iridium catalysts or even for graphene-based hybrid catalyst.<sup>3,4</sup>

Additionally, all the materials exhibited the same appearance in terms of number of layers and interlayer distances compared to their parent carbon nanotubes (see the ESI), which indicates that functionalization has not caused any damage to the nanotube layers.

The amount of the iridium in the nanotubes, determined by means of ICP-MS, varies progressively from 3.1 % for the less oxidized material, **CNT-HCl-MI-Ir**, until 12.3 % for the most oxidized material, **CNT-ST-MI-Ir** (6.1 % for **CNT-LT-MI-Ir**, and 10.0 % for **CNT-MT-MI-Ir**, Table 1). The nitrogen weight percentages determined from the TGA curves allow for the calculation of the maximum iridium load in the **CNT-X-MI-Ir** materials assuming that each imidazole-2-ylidene is involve in the formation of an Ir-NHC bond. The ratio between the iridium found and the maximum calculated is 48 %, 71 % and 98 % for **CNT-HCl-MI-Ir**, **CNT-LT-MI-Ir**, and **CNT-ST-MI-Ir**, respectively, although a slight metal overload (106 %) was found for **CNT-MT-MI-Ir**. In this context, it is worth mentioning that the iridium load could be in some way influenced by a poor dispersion capacity of the materials in the polar reaction media, together with the accessibility to the reactive acyl chloride groups.<sup>33</sup>

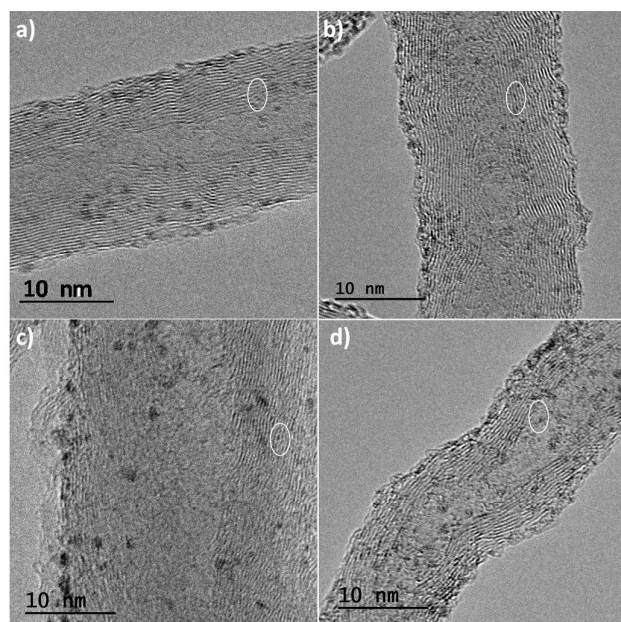


**Fig 2.** HRTEM images of the carbon nanotube-NHC-iridium hybrid catalysts: a) CNT-HCl-MI-Ir, b) CNT-LT-MI-Ir, c) CNT-MT-MI-Ir, d) CNT-ST-MI-Ir

### Structural features of the carbon nanotube-NHC-iridium hybrid catalysts

In order to gain an insight into the local structure of the iridium atoms in the hybrid catalysts, XAS measurements were performed at room temperature. Fig. 3 presents the  $\kappa^2$ -weighted EXAFS signals for all new CNT-X-MI-Ir acetyl hybrid catalysts and the known CNT-ST-1E-Ir ester hybrid catalyst<sup>3,34</sup> compared to [IrCl(cod)(Melm(CH<sub>2</sub>)<sub>3</sub>OH)] as reference compound. The hybrid catalysts show similar oscillations in the spectra though a higher damping is observed in the signal of CNT-ST-MI-Ir. The main difference between the catalysts and the reference is the clear interference at  $k \sim 8-11 \text{ \AA}^{-1}$  in the latter compound which is absent in the hybrid catalysts. This interference is ascribed to the Ir-Cl bond in the first coordination shell<sup>2,3</sup> and its absence in the catalysts' spectra suggests that the Cl has been replaced by a light element as was observed in similar catalysts.<sup>35</sup> Fig. 4a shows the pseudo radial distribution obtained from the Fourier transform (FT) of the previous EXAFS spectra between  $3.0$  and  $13.3 \text{ \AA}^{-1}$  using a Hanning window. The hybrid catalysts show a big single peak corresponding to the first coordination shell at  $R \sim 1.7 \text{ \AA}$  (without phase shift correction). The [IrCl(cod)(Melm(CH<sub>2</sub>)<sub>3</sub>OH)] reference compound instead, shows an additional shoulder at  $2.1 \text{ \AA}$  in agreement with the contribution of the Ir-Cl bond. The intensity of the main peak is similar for all catalysts with the exception of CNT-ST-MI-Ir whose peak is smaller in agreement with the high damping of the EXAFS signal. Structures beyond  $2.2 \text{ \AA}$  correspond to mixed contributions from the next-neighbours coordination shells. The peaks are significantly weaker and broader suggesting a strong disorder in these shells. Therefore, EXAFS analysis was limited to the first

coordination shell, performing the study between  $1.1$  and  $2.3 \text{ \AA}$  in the R-space.

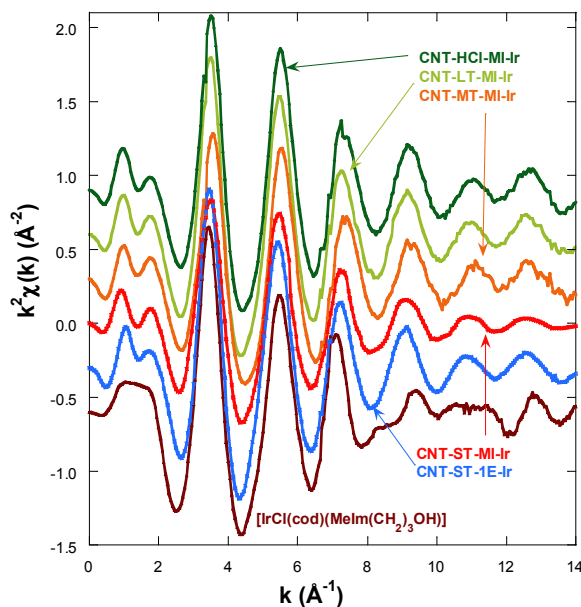


**Fig 3.**  $\kappa^2$ -weighted EXAFS spectra for the hybrid catalysts and the [IrCl(cod)(Melm(CH<sub>2</sub>)<sub>3</sub>OH)] reference compound. Data are shifted in the vertical scale for the sake of comparison.

The first coordination shell of the Ir atom in the reference compound, [IrCl(cod)(Melm(CH<sub>2</sub>)<sub>3</sub>OH)], as it was previously reported<sup>35</sup> is composed of a Cl atom, a C atom of the imidazol-2-ylidene (C<sub>1</sub>) ring and 4 C atoms of both C=C bonds present in the cyclooctadiene ligand (Fig. 5a). Our analysis yields the following distances: Ir-Cl =  $2.369(9) \text{ \AA}$ , Ir-C<sub>1</sub> =  $2.016(14) \text{ \AA}$ , Ir-C<sub>2,3</sub> =  $2.089(13) \text{ \AA}$  and Ir-C<sub>3,4</sub> =  $2.120(13) \text{ \AA}$ . The four later distances correspond to the interatomic distances to the 1,5-cyclooctadiene carbons while C<sub>1</sub> refers to the carbon atom belonging to the NHC carbene. In contrast, the Cl atom is missed in the Ir coordination shell of the supported catalysts and it is probably substituted with an O atom from the oxidized CNT materials.

In order to model the Ir local environment in the catalysts, we have replaced the Cl atom by oxygen, preserving the rest of Ir-C bonds. In fact, the Ir-O distance was matched to Ir-C<sub>1</sub> bond length because this approach strongly stabilizes the fitting procedure and minimizes the number of free parameters. Moreover, it agrees with isostructural compounds like [Ir(NCCH<sub>3</sub>)(cod)(Melm(CH<sub>2</sub>)<sub>3</sub>OH)][BF<sub>4</sub>], whose molecular structure, determined by X-ray diffraction (Fig. 5b), shows a N atom of the acetonitrile ligand bonded at  $2.032(3) \text{ \AA}$  while the Ir-C<sub>1</sub> bond length is  $2.031(3) \text{ \AA}$ .<sup>35</sup> We have observed a strong correlation between the values of Ir-C<sub>2,3</sub> and Ir-C<sub>4,5</sub>, therefore these interatomic distances were refined with a single parameter ( $\Delta R_2$ ) starting from the theoretical value of the reference compound. Therefore, a total of 4 parameters are refined: an

average inner potential correction of the threshold ( $\Delta E_0$ ), an average Debye-Waller factor ( $\sigma^2$ ) and two distances parameters,  $\Delta R_1$  for Ir-C<sub>1</sub> and Ir-O, and  $\Delta R_2$  for Ir-C<sub>2,3</sub> and Ir-C<sub>4,5</sub>. The amplitude reduction factor  $S_0^2$  is fixed to 1 in agreement with the value obtained for the reference compounds and previous studies.

Fig. 4a compares the best fit and experimental spectra corresponding to the moduli of the FTs of the  $k^2$ -weighted EXAFS shown in Fig. 3. Figure 4b shows back-Fourier filtered spectra in  $k$ -space corresponding to the first coordination shell together to the best fit results. These best fit results for **CNT-XMI-Ir** and **CNT-ST-1E-Ir**<sup>34</sup> are summarized in Table 2. Our analysis confirms a local environment composed by six light elements around the Ir atom in all the hybrid catalysts. The distances of Ir to the carbons in the diolefin range between 2.078 and 2.22 Å while the shortest distances are between 2.025 and 2.045 Å. Finally, the higher value of Debye-Waller factor is observed for **CNT-MT-MI-Ir** and especially for **CNT-ST-MI-Ir** suggesting a stronger structural disorder in the first coordination shell for these catalysts.

potential correction, bond lengths, average Debye-Waller factor and a residual factor of the fit.<sup>a</sup>

Catalyst	$\Delta E_0$ (eV)	$R_1$ (Å)	Ir-C <sub>2,3</sub> (Å)	Ir-C <sub>4,5</sub> (Å)	$10^3 \cdot \sigma^2$ (Å <sup>2</sup> )	$R_F$
<b>CNT-HCI-MI-Ir</b>	8.9(9)	2.025(16)	2.104(13)	2.190(13)	1.6(9)	0.004
<b>CNT-LT-MI-Ir</b>	9.0(9)	2.037(16)	2.114(14)	2.199(14)	1.7(9)	0.006
<b>CNT-MT-MI-Ir</b>	8.8(9)	2.033(63)	2.078(53)	2.164(53)	4.0(30)	0.014
<b>CNT-ST-MI-Ir</b>	8.8(9)	2.046(12)	2.118(11)	2.204(11)	5.0(30)	0.011
<b>CNT-ST-1E-Ir</b>	9.3(9)	2.045(13)	2.135(11)	2.221(11)	1.1(9)	0.005

<sup>a</sup> The residual factor accounts for the misfit between the actual data and the theoretical calculations.<sup>25</sup> Numbers in parentheses are the errors estimated from different analysis to the best significant digit.  $R_1$  stands for Ir-C<sub>1</sub> and Ir-O.

**Table 2.** Best fit structural parameters for the first coordination shell of the hybrid catalysts at the Ir L3-edge: Average inner

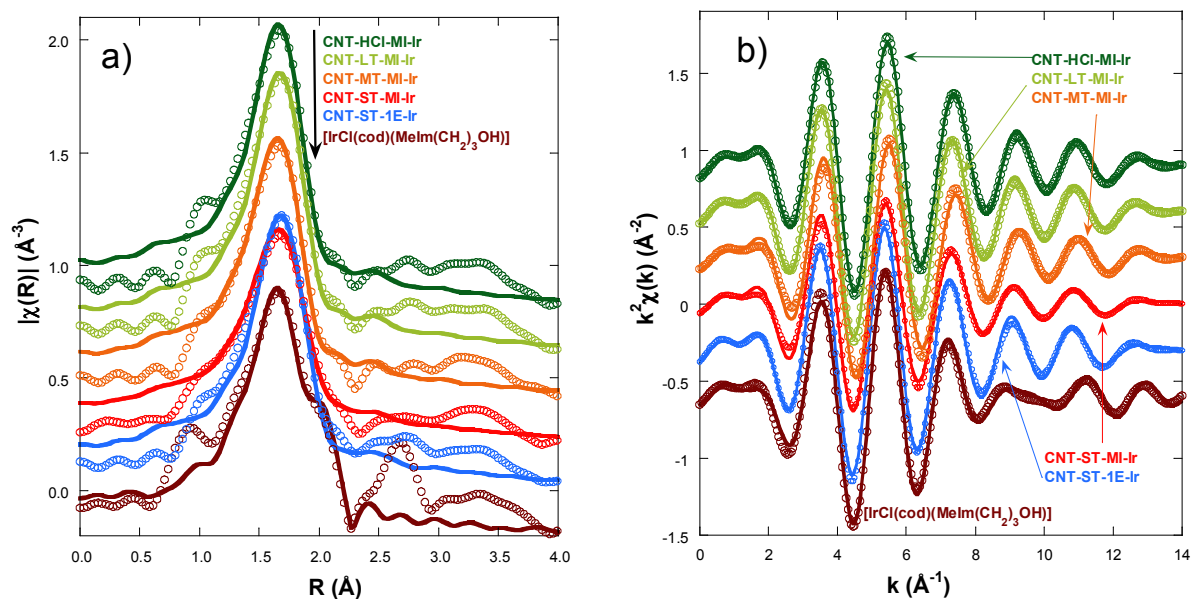


**Fig 4.** a) Fits (lines) of the Fourier transform signal (points) from  $k^2$ -weighted EXAFS signal (points) of catalysts and the reference neutral chloride compound  $[\text{IrCl}(\text{cod})(\text{Melm}(\text{CH}_2)_3\text{OH})]$  until  $R = 2.3$  Å. b) Fits (lines) of the real part of the Fourier-filtered spectra (points) between  $R=1-2.3$  Å for the same samples in  $k$ -space.

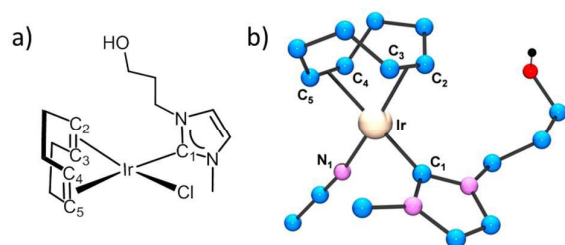
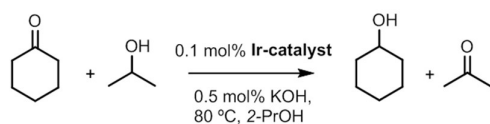


**Fig 5.** a) Schematic molecular structure of the reference neutral chloride compound  $[\text{IrCl}(\text{cod})(\text{Melm}(\text{CH}_2)_3\text{OH})]$ . b) Molecular structure of the cation of  $[\text{Ir}(\text{NCCH}_3)(\text{cod})(\text{Melm}(\text{CH}_2)_3\text{OH})][\text{BF}_4]$  (Hydrogen atoms have been omitted for clarity). Selected bond lengths (Å) and angles ( $^\circ$ ): Ir-C(1) 2.031(3), Ir-C(2) 2.127(3), Ir-C(3) 2.134(4), Ir-C(4) 2.199(3), Ir-C(5) 2.186(3), Ir-N(1) 2.032(3), C(1)-Ir-N(1) 92.44(12), C(1)-Ir-C(2) 90.58(13), N(1)-Ir-C(5) 87.55(12), C(2)-Ir-C(4) 90.11(14).

#### Hydrogen-transfer catalytic activity of the carbon nanotube-NHC-Iridium hybrid catalysts

Once the anchoring of Ir-NHC organometallic complexes on the inner and outer surfaces of the nanotubes was confirmed, the hybrid materials were tested as catalysts in the hydrogen-transfer reduction of cyclohexanone to cyclohexanol, using 2-propanol both as hydrogen source and as a non-toxic solvent with a moderate boiling point (Scheme 2). The reaction conditions were those previously optimized for related O-functionalized NHC iridium(I) homogeneous catalysts as  $[\text{IrBr}(\text{cod})(\text{Melm}(2\text{-methoxybenzyl}))]$  in previous works.<sup>2</sup> Thus, standard catalyst loads of 0.1 mol % of Ir, with 0.5 mol % of KOH as co-catalyst, and 80 °C were routinely employed.



**Scheme 2.** Transfer hydrogenation of cyclohexanone with 2-propanol.

The hybrid catalysts derived from gradually oxidized carbon nanotubes having anchored Ir-NHC complexes via acetyl linkers (**CNT-X-MI-Ir**) were active in the transfer hydrogenation of cyclohexanone. Reaction times required reaching conversion over 90% and the turnover frequencies (TOF), at initial time and at 50% conversion, for all the examined catalysts are summarized in Table 3. The four hybrid materials showed similar kinetic profiles, but

appreciable differences in the catalytic activity were found (Fig. 6a). Interestingly, the cyclohexanone reduction was observed immediately after the thermal equilibration of the reactant mixture with no detectable induction period. The hybrid catalyst **CNT-ST-MI-Ir** is the most active in this series reaching a 91% of conversion in 1.6 h with a  $\text{TOF}_{50}$  of  $3000 \text{ h}^{-1}$ . **CNT-MT-MI-Ir**, **CNT-LT-MI-Ir** and **CNT-HCl-MI-Ir** were considerably less active with  $\text{TOF}_{50}$  values of 789, 428 and  $254 \text{ h}^{-1}$ , although **CNT-MT-MI-Ir** showed an initial  $\text{TOF}_0$  of  $6500 \text{ h}^{-1}$  which is the highest in the series.

The pattern of catalytic activity shown by these hybrid catalysts **CNT-X-MI-Ir** correlates with the oxidation degree of the corresponding parent carbon nanotubes which points to a surface effect derived from the intensity of the oxidizing treatment. In fact, according to the solid characterization techniques, those supports treated with weaker oxidizing purification procedures (HCl, LT and MT treatments) result in supports with an extended  $\text{sp}^2$  structure with higher C/O ratios, low intrinsic porosity and tips scarcely opened. The low level of hydrophilic functional groups could also imply a lower dispersion capacity in the polar catalytic reaction medium which difficult the access of the reactants to the active sites, and in particular, to those settled in the inner cavity of the nanotube. On the other hand, the severe oxidation treatment (ST treatment in particular) leads to a nanotube with a defective structure, plenty of holes, oxygen moieties, structural defects and opened tips.<sup>36,37</sup> The defective structures contain suitable functional groups exposed to form active centres situated in the holes and open channels where reactants can arrive more easily in the diffusional stages of the heterogeneous catalytic process. Under these circumstances, the nanotube also can act as a “nano-reactor” offering a confinement effect that occasionally can enhance the catalysis activity.<sup>38,39,40</sup>

**Table 3.** Catalytic hydrogen transfer reduction of cyclohexanone using carbon nanotube based iridium-NHC hybrid catalysts and the related acetoxy-functionalized homogeneous catalyst  $[\text{IrCl}(\text{cod})(\text{Melm}(\text{CH}_2)_3\text{OCOCH}_3)]$  (**Ir-ImidO**).<sup>a,b</sup>

Catalyst	Time (min)	Conv (%)	$\text{TOF}_0 (\text{h}^{-1})^c$	$\text{TOF}_{50} (\text{h}^{-1})^d$
<b>CNT-HCl-MI-Ir</b>	900	91	1050	250
<b>CNT-LT-MI-Ir</b>	300	93	1500	430
<b>CNT-MT-MI-Ir</b>	200	90	6500	790
<b>CNT-ST-MI-Ir</b>	100	91	5400	3000
<b>CNT-ST-1E-Ir</b>	80	94	6300	3350
<b>CNT-ST-1C-Ir</b>	210	89	3000	1300
<b>TRCNT-ST-1C-Ir</b>	100	92	6000	3000
<b>Ir-ImidO</b>	200	94	3000	1500

<sup>a</sup> Reaction conditions: catalyst/substrate/KOH ratio of 1/1000/5, 0.1 mol% of catalyst in 2-propanol (5 mL) at 80 °C. <sup>b</sup> The reactions were monitored by GC

using mesitylene as internal standard.  $^{c,d}$  TOFs, turnover frequency [(mol product/mol catalyst)/time (h)], were calculated at initial time (60s) or at 50% of conversion,  $TOF_0$ , and  $TOF_{50}$ , respectively.

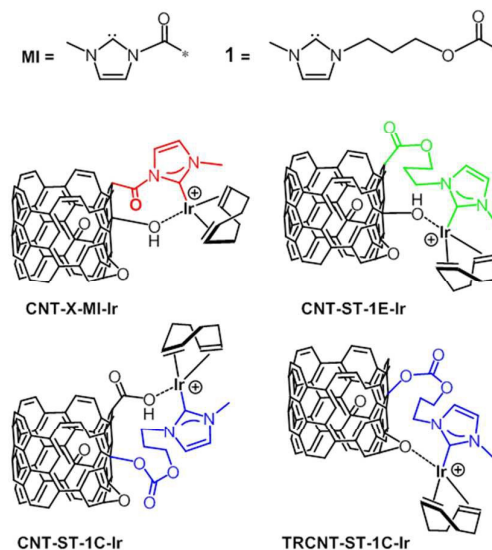
The molecular complex  $[IrCl(cod)(MelmCOCH_3)]$  has revealed as extremely moisture and alcohol sensitive which precluded the comparison of its catalytic activity with that of the carbon nanotube-NHC-iridium hybrid catalysts.  $[IrCl(cod)(MelmCOCH_3)]$  is formed in the reaction of  $[Ir(\mu-Ome)(cod)]_2$  with the corresponding N-acetyl imidazolium salt along with complex  $[IrCl(cod)(MelmH)]$  resulting from the methanolysis of the acyl fragment. In fact,  $[IrCl(cod)(MelmCOCH_3)]$  was cleanly converted to  $[IrCl(cod)(MelmH)]$  and methyl acetate upon reaction with methanol (NMR evidence).

It is noteworthy that neither the iridium-free carbon nanotube-based materials nor iridium supported materials without imidazolium ligand have shown significant catalytic activity, which indirectly supports the covalently anchoring of the Ir-NHC complexes to the carbon nanotube-based materials via acetyl linkers. In this context, it has been recently reported that iridium oxide nanoparticles supported on nanoparticulate cerium oxide exhibit moderate catalytic activity in the transfer hydrogenation of cyclohexanone.<sup>41</sup> However, the presence of  $IrO_2$  nanoparticles in our NHC-Ir hybrid catalysts is negligible because of the fit the first shell of our EXAFS spectra to a model with a rutile crystal structure ( $IrO_2$ ) render a poor model. In fact, the EXAFS signal of  $IrO_2$  shows some structures in the oscillation between 7 and 9  $\text{\AA}^{-1}$  that are lacked in the spectra or our catalysts, the Fourier transform shows an important peak below 3  $\text{\AA}$  corresponding to the Ir-Ir path that is also absent in our spectra, and the white line (very sensitive to the number of d-holes) is significant higher for the  $IrO_2$  spectrum.<sup>42</sup>

The catalytic performance of **CNT-ST-MI-Ir** has been compared with that of the molecular acetoxy-functionalized NHC complex  $[IrCl(cod)(Melm(CH_2)_3OCOCH_3)]$  (**Ir-Imido**),<sup>3</sup> and of related hybrid catalysts having supported Ir-NHC complexes on carbon nanotubes obtained under the most severe oxidizing conditions through the flexible 3-alkoxypropyl linker **1**. In particular, the hybrid catalysts **CNT-ST-1E-Ir**<sup>3</sup> and **CNT-ST-1C-Ir**, with ester and carbonate linking surface functions resulting from the nanotube functionalization through the carboxylic acid and the hydroxyl surface groups, respectively, whereas **TRCNT-ST-1C-Ir** comes from the surface hydroxylic groups functionalization of thermally reduced nanotubes (Scheme 3).<sup>35</sup>

As can be observed in Figure 6b, the hybrid catalyst **CNT-ST-1E-Ir** is only slightly more active than **CNT-ST-MI-Ir** reaching a 94% of conversion in 1.3 h with a  $TOF_{50}$  of 3350  $h^{-1}$  (Table 3). Thus, the flexibility imparted by the carbon chain linking the Ir-NHC supported complexes in **CNT-ST-1E-Ir** appears to influence positively the catalytic activity as both hybrid catalysts have a similar degree of oxidation. Interestingly, both hybrid catalyst are more active than the homogeneous catalyst  $[IrCl(cod)(Melm(CH_2)_3OCOCH_3)]$  (**Ir-Imido**) and the hybrid catalysts

prepared by covalent functionalization of the hydroxyl surface groups **CNT-ST-1C-Ir** and **TRCNT-ST-1C-Ir** (Figure 6b).



**Scheme 3.** Carbon nanotube based iridium-NHC hybrid catalysts.

In contrast with the hybrid catalysts **CNT-X-MI-Ir**, for which the catalytic performance improve with the level of the oxidation of the parent carbon nanotube material, the thermally reduced **TRCNT-ST-1C-Ir** was found to be more active than **CNT-ST-1C-Ir** (Figure 6b).<sup>35</sup> The structural characterization of the catalysts based on thermally reduced carbon nanotube materials showed an increase in the amount of  $Csp^2$  and a decrease in the oxygen functional groups, as a consequence of the partial restoring of the aromatic structure after the thermal treatment. Having in mind that EXAFS measurements showed a similar first-neighbours coordination shells for all the hybrid Ir-NHC catalysts,<sup>35</sup> that difference should be ascribed to the different localization of the iridium centres in the hybrid catalysts. The active centres are located at the basal planes of the nanotubes for the catalyst with  $-OH$  functionalization, while for the  $-COOH$  functionalized materials, the Ir-NHC complexes are located at the holes and defects, where the approach of the reactants is easier because these centres are more exposed. However, in the case of a cleaner surface, what is provided for the thermal reduction, the diffusional stages can be faster, which enhances the activity of the reduced samples. That observations could be of a great importance because gives a clear idea of how should be the functionalization in order to get more active catalysts.

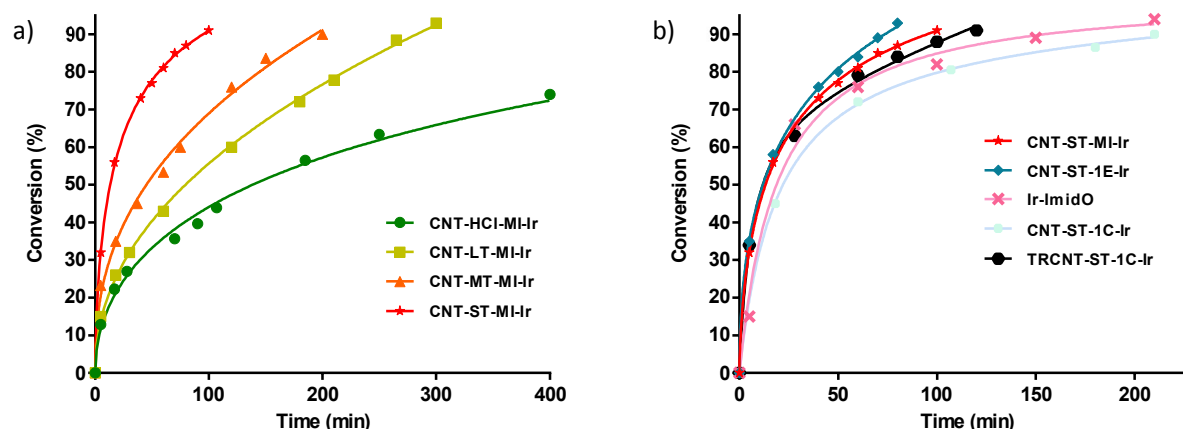


**Fig 6.** Reaction profiles for the transfer hydrogenation of cyclohexanone (%) with 2-propanol by carbon nanotube based iridium-NHC hybrid catalysts (0.1 mol % of Ir) at 80 °C. a) Cyclohexanone reduction by **CNT-X-MI-Ir** hybrid catalysts. b) Cyclohexanone reduction by **CNT-ST-MI-Ir** compared with **CNT-ST-1E-Ir**, **CNT-ST-1C-Ir**, **TRCNT-ST-1C-Ir**, and the homogeneous  $[\text{IrCl}(\text{cod})(\text{Melm}(\text{CH}_2)_3\text{OCOCH}_3)]$  (**Ir-ImidO**) catalyst. Continuous lines represent a mathematical fit with the experimental data points.

Recycling studies (Fig. 7) were also carried out with the four hybrid catalysts **CNT-X-MI-Ir** based on gradually oxidized carbon nanotubes. The black solids obtained after each catalytic run were recovered, washed with fresh 2-propanol (4-5 mL) and subjected to another catalytic cycle. The recycling processes render conversions above 90% after five catalytic runs without any loss of catalytic activity. In addition, the kinetic profiles in the successive experiments are very similar to those plotted on Fig. 6a, even for the last cycle which was performed on air, which demonstrate the air stability of the hybrid catalysts.<sup>3,35</sup> (see the ESI).

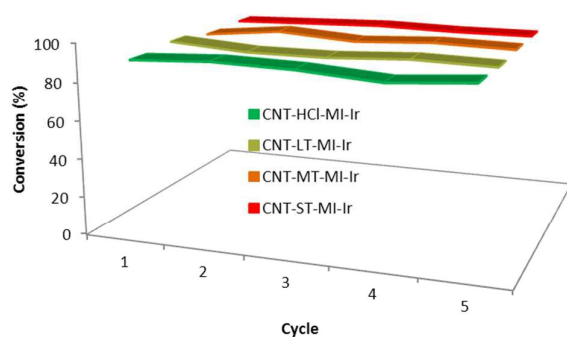


**Fig 7.** Recyclability of the hybrid catalysts **CNT-X-MI-Ir**: conversion to cyclohexanone in five catalytic runs with recycling reaction times of Table 3. The 5<sup>th</sup> was performed under air.

## Conclusions

Iridium N-heterocyclic carbene complexes have been supported through the surface carboxylic acid groups of carbon nanotube materials obtained after purification methods of different oxidizing power. The oxidized carbon nanotubes have been functionalized by reaction of the surface acyl chloride groups formed after thionyl chloride treatment with N-methylimidazole, which allow for the covalent anchoring of Ir-NHC complexes via acetyl linkers. The carbon nanotube based iridium-NHC hybrid materials, **CNT-X-MI-Ir**, were efficient catalysts for the reduction of cyclohexanone by transfer hydrogenation. The most oxidized hybrid catalyst **CNT-ST-MI-Ir** has shown a superior catalytic performance, observing a gradual increase of the catalytic activity with the oxidation degree of the corresponding parent carbon nanotubes. The supported catalysts can be recycled through successive catalytic runs without any loss of activity.

In sharp contrast with the behaviour exhibited by a related N-acyl-substituted Ir-NHC molecular complex, the catalytic activity exhibited by the iridium hybrid catalysts suggests that the acetyl linkers in these materials do not undergo methanolysis under hydrogen transfer conditions which could be a consequence of the protection and stabilizing effect exerted by the nanocarbon walls of the support.

The local structure of the iridium atoms in the hybrid catalyst determined by EXAFS has shown a common local environment for all of them implying a coordination iridium sphere formed by two olefin bonds of the cod ligand, the carbon atom of the NHC carbene ligand, and an O atom from

the oxidized carbon matrix as a result of the iridium-support interaction after ionization of the chlorido ligand.

The covalent functionalization through carboxylic acid moieties in the hybrid Ir-NHC catalyst makes possible both a confinement effect due to the porosity of the material and a surface effect based on the potential cooperation of hydroxyl functional groups on the nanotube walls. In this context, it has been found that the catalytic activity is enhanced by the presence of a high concentration of oxygen functionalities in the periphery of the active centers predominantly located at the structural defects including holes or opened tips.

### Acknowledgements

The authors thank the Spanish Ministry of Economy and Competitiveness (MINECO/FEDER) (Projects Consolider Ingenio 2010 CSD2009-00050 and CTQ2013-42532-P), and the Diputación General de Aragón (FSE-E07 and FSE-E69) for their financial support. Dr. P. A. thanks MINECO for a Ramón y Cajal contract. M. B. acknowledges his fellowship from MECO (AP2010-0025). The authors also thank Dr. Gloria Subías for fruitful discussion in the EXAFS analysis.

### Notes and references

† Footnotes

- a) F. E. Hahn and M. C. Jahnke, *Angew. Chem. Int. Ed.*, 2008, **47**, 3122–3172; b) C. M. Crudden and D. P. Allen, *Coord. Chem. Rev.*, 2004, **248**, 2247–2273; c) W. A. Herrmann, *Angew. Chem. Int. Ed.*, 2002, **41**, 1290–1309.
- M. V. Jiménez, J. Fernández-Tornos, J. J. Pérez-Torrente, F. J. Modrego, S. Winterle, C. Cunchillos, F. J. Lahoz and L. A. Oro, *Organometallics*, 2011, **30**, 5493–5508.
- a) M. Blanco, P. Álvarez, C. Blanco, M. V. Jiménez, J. Fernández-Tornos, J. J. Pérez-Torrente, L. A. Oro and R. Menéndez, *ACS Catal.*, 2013, **3**, 1307–1317; b) M. Blanco, P. Álvarez, C. Blanco, M. V. Jiménez, J. Fernández-Tornos, J. J. Pérez-Torrente, L. A. Oro and R. Menéndez, *Carbon*, 2015, **83**, 21–31.
- a) S. Sabater, J. A. Mata and E. Peris, *Organometallics*, 2015, **34**, 1186–1190; b) S. Sabater, J. A. Mata and E. Peris, *ACS Catalysis*, 2014, **4**, 2038–2047; c) Q. Zhao, Y. Li, R. Liu, A. Chen, G. Zhang, F. Zhang and X. Fan, *J. Mater. Chem. A*, 2013, **1**, 15039–15045; d) Q. Zhao, C. Bai, W. Zhang, Y. Li, G. Zhang, F. Zhang and X. Fan, *Ind. Eng. Chem. Res.*, 2014, **53**, 4232–4238; e) G. Liu, B. Wu, J. Zhang, X. Wang, M. Shao, J. Wang, *Inorg. Chem.*, 2009, **48**, 2383–2390.
- S. Iijima, *Nature*, 1991, **354**, 56–58.
- C. T. White and T. N. Todorov, *Nature*, 1998, **393**, 240–242.
- J. P. Lu, *Phys. Rev. Lett.*, 1997, **79**, 1297–1300.
- J. Zhao and R. H. Xie, *J. Nanosci. Nanotechnol.*, 2003, **3**, 459–462.
- M. Wilson, K. Kannagaram, G. Smith and B. Raguse, in *Nanotechnology. Basic Science and Emerging Technologies*. CRC Press, London, 2002.
- S. Porro, S. Musso, M. Vinante, L. Vanzetti, M. Anderle, F. Trotta and A. Tagliaferro, *Physica E: Low-dimensional Systems and Nanostructures*, 2007, **37**, 58–61.

- A. Aqel, K. M. M. A. El-Nour, R. A. A. Ammar and A. Al-Warthan, *Arab. J. Chem.*, 2012, **5**, 1–23.
- G. G. Wildgoose, P. Abiman and R. G. Compton, *J. Mater. Chem.*, 2009, **19**, 4875–4886.
- a) K. Krishnamoorthy, M. Veerapandian, K. Yun and S. -J. Kim, *Carbon*, 2013, **53**, 38–49; b) V. Datsyuk, M. K. K. Papagelis, J. Parthenios, D. Tasis, A. Siokou, I. Kallitsis and C. Galiotis, *Carbon*, 2008, **46**, 833–840.
- J. Zhang, H. Zou, Q. Qing, Y. Yang, Q. Li, Z. Liu, X. Guo and Z. Du, *J. Phys. Chem. B.*, 2003, **107**, 3712–3718.
- F. Avilés, J. V. Cauich-Rodríguez, L. Moo-Tah, A. May-Pat and R. Vargas-Coronado, *Carbon*, 2009, **47**, 2970–2976.
- A. G. Osorio, I. C. L. Silveira, V. L. Bueno and C. P. Bergmann, *Appl. Surf. Sci.*, 2008, **255**, 2485–2489.
- M. N. Hopkinson, C. Richter, M. Schedler and F. Glorius, *Nature*, 2014, **510**, 485–495.
- A. C. Hillier, H. M. Lee, E. D. Stevens and S. P. Nolan, *Organometallics*, 2001, **20**, 4246–4252.
- D. Wang and D. Astruc, *Chem. Rev.* 2015, **115**, 6621–6686.
- a) M. R. Axet, O. Dechy-Cabaret, J. Durand, M. Gouygou and P. Serp, *Coord. Chem. Rev.*, DOI:10.1016/j.ccr.2015.06.005; b) I. Romanenko, D. Gajan, R. Sayah, D. Crozet, E. Jeanneau, C. Lucas, L. Leroux, L. Veyre, A. Lesage, L. Emsley, E. Lacôte and C. Thieuleuxet, *Angew. Chem., Int. Ed.*, 2015, **54**, 12937–12941; c) Y. Yan, J. Miao, Z. Yang, F.-X. Xiao, H. B. Yang, B. Liu and Y. Yang, *Chem. Soc. Rev.*, 2015, **44**, 3295–3346; d) L. Zhang, E. Castillejos, P. Serp, W. Sun, J. Durand, *Cat. Today*, 2014, **235**, 33–40; e) A. Schaez, M. Zeltner, and W. J. Stark, *ACS Catal.* 2012, **2**, 1267–1284.
- a) G. E. Dobreiner, C. A. Chamberlin, N. D. Schley and R. H. Crabtree, *Organometallics*, 2010, **29**, 5728–5731; b) B. Bovio, A. Burini and B. R. Pietroni, *J. Organomet. Chem.*, 1993, **452**, 287–291; b) M. Jonek, A. Makhlofi, P. Rech, W. Frank and C. Ganter, *J. Organomet. Chem.*, 2014, **750**, 140–149; c) R. A. Batey, M. Shen, A. J. Lough, *Org. Lett.* 2002, **4**, 1411–1414.
- R. Usón, L. A. Oro and J. A. Cabeza, *Inorg. Synth.*, 1985, **23**, 126–127.
- P. M. A. Sherwood, in *Practical Surface Analysis in Auger and X-ray Photoelectron Spectroscopy*, eds. D. Briggs and M. P. Seah, Wiley, New York, 1990, Vol. 1, pp. 574.
- D. Elgrabli, M. Floriani, S. Abella-Gallart, L. Meunier, C. Gamez, P. Delalain, F. Rogerieux, J. Boczkowski and G. Lacroix, *Part. Fibre Toxicol.*, 2008, **5**, 20–33.
- B. Ravel and M. Newville, *J. Synchrotron Radiat.*, 2005, **12**, 537–541.
- J. J. Rehr and R. C. Albers, *Rev. Mod. Phys.*, 2000, **72**, 621–654.
- M. Blanco, P. Álvarez, C. Blanco, N. Campos, D. Gómez and R. Menéndez, *Diam. Relat. Mater.*, 2013, **37**, 1–7.
- Y. C. Chiang, W. H. Lin and Y. C. Chang, *Appl. Surf. Sci.*, 2011, **257**, 2401–2410.
- M. S. Dresselhaus, G. Dresselhaus, R. Saito and A. Jorio, *Phys. Rep.*, 2005, **409**, 47–99.
- M. J. Park, J. K. Lee, B. S. Lee, Y. W. Lee, I. S. Choi and S. Lee, *Chem. Mater.*, 2006, **18**, 1546–1551.
- C. Crotti, E. Farnetti, S. Filipuzzi, M. Stener, E. Zangrando and P. Moras, *Dalton Trans.*, 2007, 133–142.
- J. Lu, P. Serna, C. Aydin, N. D. Browning and B. C. Gates, *J. Am. Chem. Soc.*, 2011, **133**, 16186–16195.
- D. G. Rees and P. J. Halling, *Enzyme Microb. Technol.*, 2000, **27**, 549–559.
- J. Blasco, V. Cuartero, G. Subías, M. V. Jiménez, J. J. Pérez-Torrente, L. A. Oro, M. Blanco, P. Álvarez, C. Blanco and R. Menéndez, *J. Phys.: Confer. Series*, accepted, 2016.

- 35 M. Blanco, P. Álvarez, C. Blanco, M. V. Jiménez, J. Fernández-Tornos, J. J. Pérez-Torrente, J. Blasco, G. Subías, V. Cuartero, L. A. Oro and R. Menéndez, *Carbon*, 2016, **96**, 66–74.
- 36 F. Su, C. Lu and S. Hu, *Colloid Surf. A*, 2010, **353**, 83–91.
- 37 F. Su, C. Lu and S. Hu, *Appl. Surf. Sci.*, 2008, **254**, 7035–7041.
- 38 X. Pan and X. Bao, *Acc. Chem. Res.*, 2011, **44**, 553–562.
- 39 R. M. Malek Abbaslou, J. Soltan and A. K. Dalai, *Appl. Catal. A-Gen.*, 2010, **379**, 129–134.
- 40 P. Serp and E. Castillejos, *ChemCatChem*, 2010, **2**, 41–47.
- 41 C. Hammond, M. T. Schümperli, S. Conrad, and I. Hermans, *ChemCatChem* 2013, **5**, 2983–2990.
- 42 E. Prouzet, *J. Phys.: Condens. Matter*. 1995, **7**, 8027–8033.

## Graphical Abstract

The hydrogen-transfer catalytic activity of hybrid carbon nanotube-based iridium-NHC catalysts is strongly influenced by the oxidation degree of the support

